Chapter 1
Residual Stresses in Bovine Femurs

Yongbo Zhang and Drew Nelson

Abstract The slitting method has become well-established for determining residual stresses in engineering materials. This study develops and applies a version of that method using a small slot to find residual stresses vs. depth in layers near the surface of bovine femurs. Results are obtained for the central region (diaphysis) of hydrated femurs from both mature and young cows. The magnitude of residual stresses was found to be greatest in thin layers near the surface, typically 100–200 μm deep. Residual stresses in those layers were compressive in mature femurs at the circumferential location tested, but tensile in hydrated young femurs.

Keywords Residual stress • Bone • Femur • Slitting method • X-ray diffraction

1.1 Introduction

The presence of residual stresses in components made of engineering materials is well known. Residual stresses and strains also exist in arteries [1–6], the esophagus [7–10], intestines [11, 12], brain [13], skin [14], etc. and may play an important role in the mechanical behavior of biological structures. For instance, at the inner diameter of arteries, compressive circumferential residual strains are believed to significantly reduce tensile stresses from blood pressure [4, 15–17] and enhance resistance to failure [18]. (The distinction between residual stresses and strains is made here because residual strains can have a different influence on the nonlinear stress-strain behavior of soft tissue than residual stresses).

The existence and possible role of residual stresses in bone does not appear to be well-understood. X-ray diffraction (XRD) has been widely applied to find residual stresses in engineering materials with crystalline structures [19]. More recently, it has been applied to bone, a major constituent of which is the mineral hydroxyapatite (HAP) [20]. In the following summary, residual stresses refer to values determined by XRD with HAP crystals serving as "miniature strain sensors." Residual stresses have been measured in specimens taken mainly from bovine femurs [21, 22–29], but also from canine fibula [30, 31] and the extremities of rabbits [32, 33]. The size and condition of specimens prior to and during experiments has varied considerably from study-to-study. A number of studies [21, 23–27] have used sizeable specimens removed from the central portion (diaphysis) of bovine femurs as depicted in Fig. 1.1 and measured residual stresses at the surface or at various depths. All but one of those studies used air dried specimens, and reported longitudinal tensile stresses, in some cases exceeding 100 MPa at the surface, with smaller values of compressive stress (≈ -10 MPa) at depths of 1 mm. Residual stresses were found to vary considerably with position around the circumference of specimens. Other studies used much smaller specimens (dimensions on the order a few mm) of bovine femurs [22, 28, 29] or canine fibula [31] that were kept hydrated. Compressive residual stresses and strains were measured through the thickness with synchrotron X-rays, with values as large as -150 MPa and -2500 με, respectively. For perspective on the magnitude of residual stress and strain values mentioned above, the longitudinal tensile yield stress of bovine femurs is approximately 100–130 MPa [20, 34]. The yield strain is estimated to be about 6500 με [35].

The interpretation of results from the XRD studies can be complicated by the following factors. Using $1 \times 1 \times 10$ mm specimens taken from bovine femurs, Tung et al. [29] found that initial compressive residual stresses (exceeding -100 MPa) became tensile after about 20 min without hydration, climbing to approximately $+75$ MPa after an hour. Measured values of residual stresses may thus be altered if dehydration occurs during XRD experiments, although the extent of that influence

Y. Zhang
Institute of Solid Mechanics, Beihang University, Beijing 100191, China

D. Nelson (✉)
Mechanical Engineering Department, Stanford University, Stanford, CA 94305, USA
e-mail: dnelson@stanford.edu

A. Baldi et al. (eds.), *Residual Stress, Thermomechanics & Infrared Imaging, Hybrid Techniques and Inverse Problems, Volume 8*,
Conference Proceedings of the Society for Experimental Mechanics Series, DOI 10.1007/978-3-319-62899-8_1

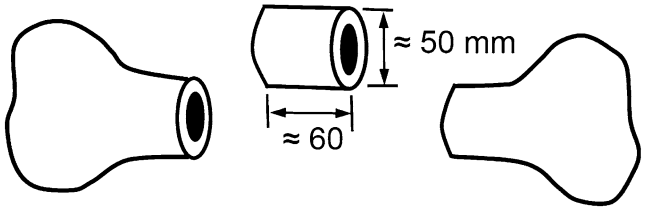

Fig. 1.1 Schematic of a specimen cut from the central portion (diaphysis) of a bovine femur

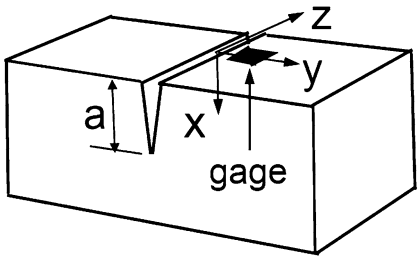

Fig. 1.2 Slitting geometry

is unknown for larger specimens. Dissecting a bone into successively smaller pieces changed values of residual stresses measured by XRD [32]. Recent studies [22, 29] have also found that compressive residual stresses in small specimens, as measured via HAP crystals, dropped significantly with radiation dose. Doses are not reported in most of the XRD studies of bone and may or may not have influenced results.

Residual stresses can also be measured in objects by releasing residual stresses, measuring resulting strains or deflections, and then using a computational model that relates the strains or deflections to the residual stresses. Stanwyck et al. [36] applied a strain gage in the longitudinal direction of a bovine metatarsal bone and sawed a 2 mm deep cut in the transverse direction of the bone, near the gage. A compressive strain of -180 με was reported. When the cut was deepened to 3 mm, the strain increased to -280 με. The area surrounding the cut was irrigated with saline solution during the sawing. This experiment could be considered an early form of the slitting method for residual stress determination. Residual stresses were not computed from the measured strains, which is understandable since the methodology to do so was in its infancy when the experiment was conducted in the early 1980s. This paper will explore a version of the slitting method adapted to find residual stress vs. depth in bovine femurs, using a refined experimental approach and a finite element model.

1.2 Slitting Method

As background, key features of the slitting method will be summarized. Suppose that a slit is introduced incrementally in depth into an object containing residual stresses σ normal to the slit and varying in an unknown manner with depth x, as depicted in Fig. 1.2. The slit releases residual stresses, causing the surface to develop strains ε normal to the slit, which are typically measured with a strain gage near the slit location (and/or on the opposite side of the object if desired). Measured strain vs. depth data can be used with a computational model to determine the variation of σ with depth [37–39]. Assuming that residual stresses are constant in the z-direction, residual stresses σ can be related to strains by [40]:

$$\epsilon\left(a_i\right) = \int_0^{a_i} G\left(x, a_i\right) \sigma\left(x\right) dx \tag{1.1}$$

where $\epsilon(a_i)$ is the measured strain when a slit is at depth a_i. The function $G(\mathrm{x}, a_i)$ gives the strain response from a unit stress at depth x for a slit of depth a_i.

Residual stresses vs. depth can approximated by

$$\sigma(x) = \sum\nolimits_{j=1}^{n} A_j \, U_j(x) \tag{1.2}$$

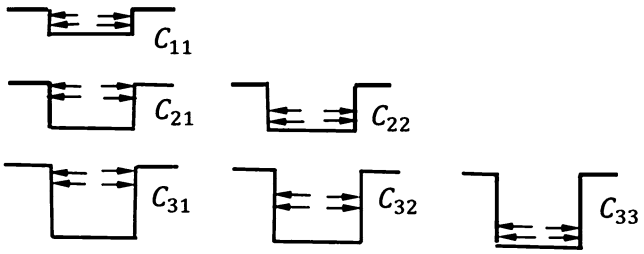

Fig. 1.3 Illustration of unit stresses applied to different increments of depth to find compliance matrix C_{ij}.

where A_j are coefficients to be found and $U_j\,(x)$ are unit pulses with $U_j\,(x) = 1$ for a depth increment $a_{j-1} \leq x \leq a_j$ and zero for $x \leq a_{j-1}, x \geq a_j$. Substituting Eq. 1.2 into Eq. 1.1 gives

$$\epsilon\,(a_i) = \sum\nolimits_{j=1}^{n} A_j C_{ij} \tag{1.3}$$

with a compliance matrix given by

$$C_{ij} = \frac{1}{E} \int_{a_j}^{a_{j-1}} G\,(x, a_i)\; U_j(x) dx \tag{1.4}$$

and $E =$ modulus of elasticity.

From Eqs. 1.1 and 1.4, the matrix elements C_{ij} represent strains at the surface from unit stresses applied to various increments of depth $a_{j-1} \leq x \leq a_j$. Values of C_{ij} can be found by a creating a finite element model of a slit and applying stresses as in Fig. 1.3.

Expressing Eq. 1.3 as $\{\epsilon\} = [\mathrm{C}]\;\{A\}$ leads to a solution for the coefficients A_j in Eq. 1.2 in terms of measured strains:

$$\{A\} = \left([C]^T\,[C]\right)^{-1}\,[C]^T\,\{\varepsilon_{\mathrm{meas}}\} \tag{1.5}$$

The determination of residual stresses vs. depth using the "unit pulse" method can be improved by Tikhonov regularization [41] to reduce effects of experimental uncertainties.

1.3 Slotting Model

The slitting method was adapted for application to the central portion of femurs by the use of a small slot as depicted in Fig. 1.4 at regions that were flat over the length of a slot. Prior to performing experiments on bone, a finite element model was developed to determine compliance coefficients *Cij* for incremental slotting. The finite element code ABAQUS was with the model shown in Fig. 1.5, which employed eight-node linear brick elements. The nodes on the bottom of the model were fixed. The slot length D was 2.6 mm and the width 2R was 0.8 mm. The width of the slit was based on the smallest diameter end mill that would not break when making a slot. The slot was extended to a depth of 0.61 mm in ten steps. Each of the first six steps was 0.051 mm, followed by four steps of 0.076 mm each. Compliance *Cij* values were computed by applying a unit stress step-by-step as illustrated in Fig. 1.3. Slot extension in depth was simulated by deleting elements. Displacement data were used to compute strains using the method in Ref. 42. Orthotropic material behavior was used in the model, with longitudinal and transverse (tangential) moduli of elasticity $\mathrm{E_L}$ and $\mathrm{E_T}$ values as described shortly, plus values for Poisson's ratios and shear moduli available for bovine femur [43]. As might be anticipated, the value of $\mathrm{E_L}$ governed strains from slotting. Experiments utilized hydrated femurs from mature (20–24 months old) and young (3–4 months old) cows. Rather than assuming that published values of $\mathrm{E_L}$ and $\mathrm{E_T}$ for bovine femurs would be applicable over the depth of slotting used here, tests were performed to find $\mathrm{E_L}$, $\mathrm{E_T}$ values relevant to that depth. Specimens with a length of 9.0 mm and a rectangular cross-section with a 1.0 mm width and 0.4–0.5 mm thickness were carefully milled from surface layers of different femurs and stored in PBS at room temperature. The specimens were tested in a miniature three point bending fixture with a span of 8.0 mm. The mid-point deflection of each specimen was monitored using a 100 power microscope. Modulus of elasticity

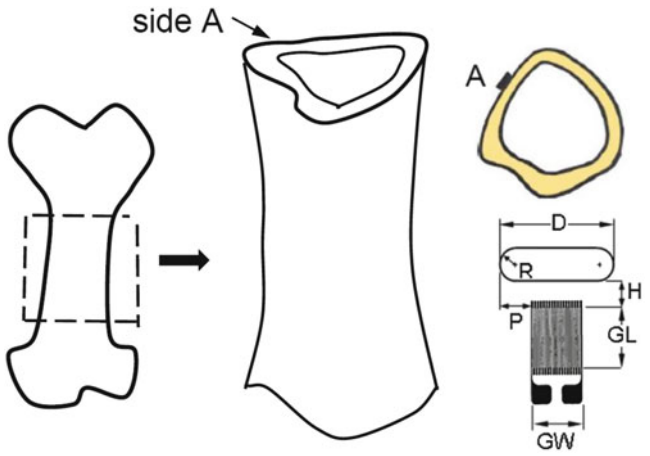

Fig. 1.4 Schematic of femur, typical specimen and a slot with adjacent strain gage (D = 2.6, R = 0.4, H = 1.0, P = 0.55, GL = 3.0, GW = 1.5 mm)

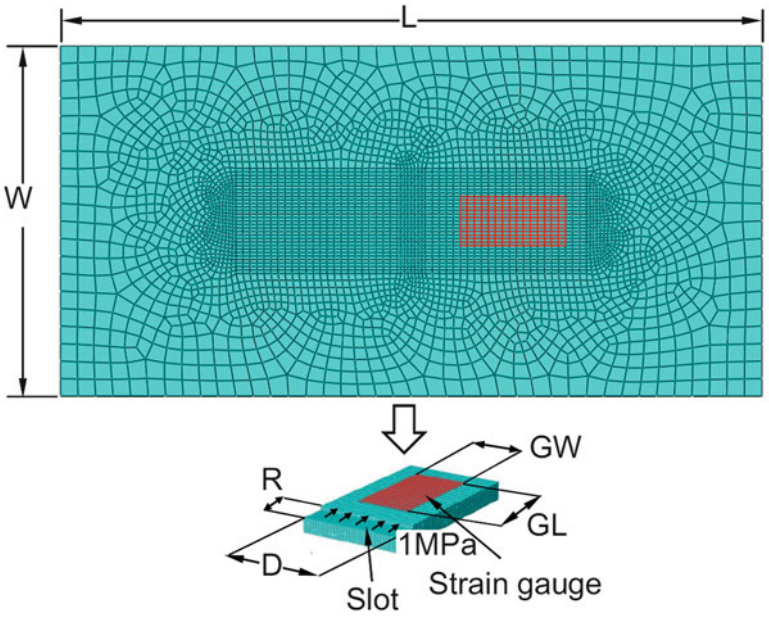

Fig. 1.5 Finite element model to simulate slotting with unit stresses applied along the straight portion of the slot

was computed from a relation between mid-point deflection and bending moment. For tests of femurs from two mature cows, average E_L and E_T were 22.0 and 9.1 GPa, respectively. The range of E_L for specimens from previous studies [34, 43–45], which used specimens roughly an order of magnitude larger than those here, was 19.3–22.6 GPa, and 12.4 to 14.6 GPa for E_T. Tests using specimens from two young cows gave average E_L and E_T of 14.6 and 8.5 GPa. Values of E_L and E_T of 6.6 and 5.3 GPa have been reported in a recent study involving young bovine femurs [45].

1.4 Slotting Experiments with Bone Specimens

Each refrigerated bovine femur (with ends removed as illustrated in Fig. 1.4) was obtained from a butcher within 24 h of slaughter. Soft tissue was removed and the resulting specimen placed in phosphate buffered saline (PBS) for 48 h. Specimens were 125–150 mm long, with cross sectional widths between 50 and 75 mm. Next, each specimen was placed in a fixture that held it steady for slotting and enabled fine adjustments of tilt in two directions. A specimen and its holding fixture were then submerged in a water tank at room temperature, and a slotting setup illustrated in Fig. 1.6 installed over the specimen.

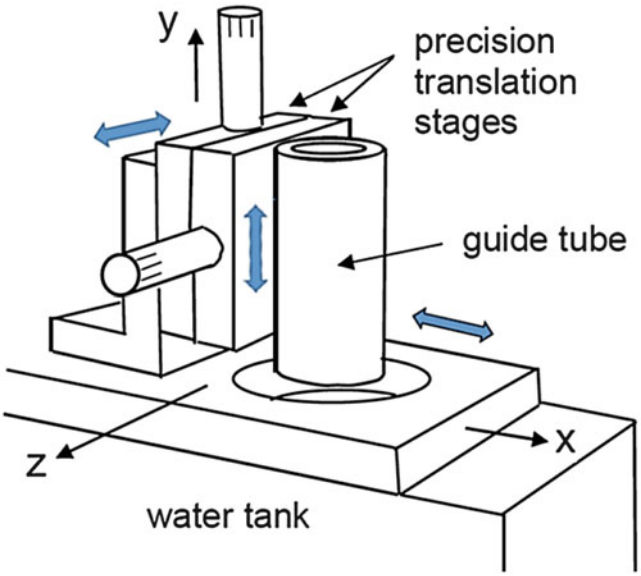

Fig. 1.6 Schematic of setup used to perform slotting experiments, adjustable in x,y,z directions

The setup enabled translation in x,y and z directions. Next, a displacement probe was slid into the guide tube and used to map the flatness of the region. Through adjustment of the location and tilt of a specimen, it was possible to identify surface regions that were on average flat to within 0.013 mm (0.0005 in.) over a prospective slot length. Those regions were marked with waterproof ink. With a specimen temporarily removed from the water tank, a strain gage was attached to the surface adjacent to a prospective slot using cyanoacrylate adhesive, which cures well in the presence of moisture. Care was taken to ensure that no adhesive extended into the region of a prospective slot. A strain gage and its terminal pad were covered with a polyurethane coating for protection from water, with the slot area masked temporarily to prevent it from being covered. After allowing 20 min for the coating to dry, a specimen was returned to the water tank and the orientation of an intended slot adjusted to ensure it was horizontal. The specimen was submerged in the water tank for 24 h for additional hydration and to allow the temperature of the specimen to equilibrate with that of the water surrounding it. Prior to making a slot, the thermal stability of strain readings was checked. Strains did not fluctuate by more than 2 $\mu\varepsilon$ over the anticipated duration of an experiment.

Slotting was performed by sliding a boring bar with an end mill into the tubular guide in Fig. 1.6. Slot depth was set using a precision translation stage (y-direction). Each slot was made by manually rotating the boring bar and gradually translating the end mill in the z direction using a second translation stage. Powered drilling has been found to damage bone tissue by heating [46] and thus gentle manual rotation (less than 10 RPM) was used in an effort to avoid such damage and its unknown effect on results of the experiments. After each slotting step, actual depth was measured at four locations along the length of a slot, and the average of those values used in expressing strain vs. depth. The actual depth after each step during slotting experiments was not exactly the same as in the finite element model. Depths were measured after each step to a resolution of 0.0025 mm (0.0001 in.). Values of strain corresponding to the depths used in the finite element model were found by interpolation from the measured strains vs. depth. Each specimen, including slot and strain gage, was submerged during the entirety of a slotting experiment. Final slot depths were close to 0.61 mm.

1.5 Initial Results

Residual stresses vs. depth as determined by slotting are shown in Fig. 1.7. Magnitudes are most significant in thin layers just beneath the surface. Compressive residual stresses near the surface were found for femurs from mature cows, while those from young cows had tensile residual stresses. The magnitudes of residual stresses found by slotting may seem insignificant at first glance. However, the magnitudes may be of more significance when noting again that the tensile yield stress of mature bovine femurs is on the order 100–130 MPa [20, 34] (and perhaps somewhat lower for young femurs). Experiments to provide residual stress data for other circumferential locations on young and mature femurs are planned.

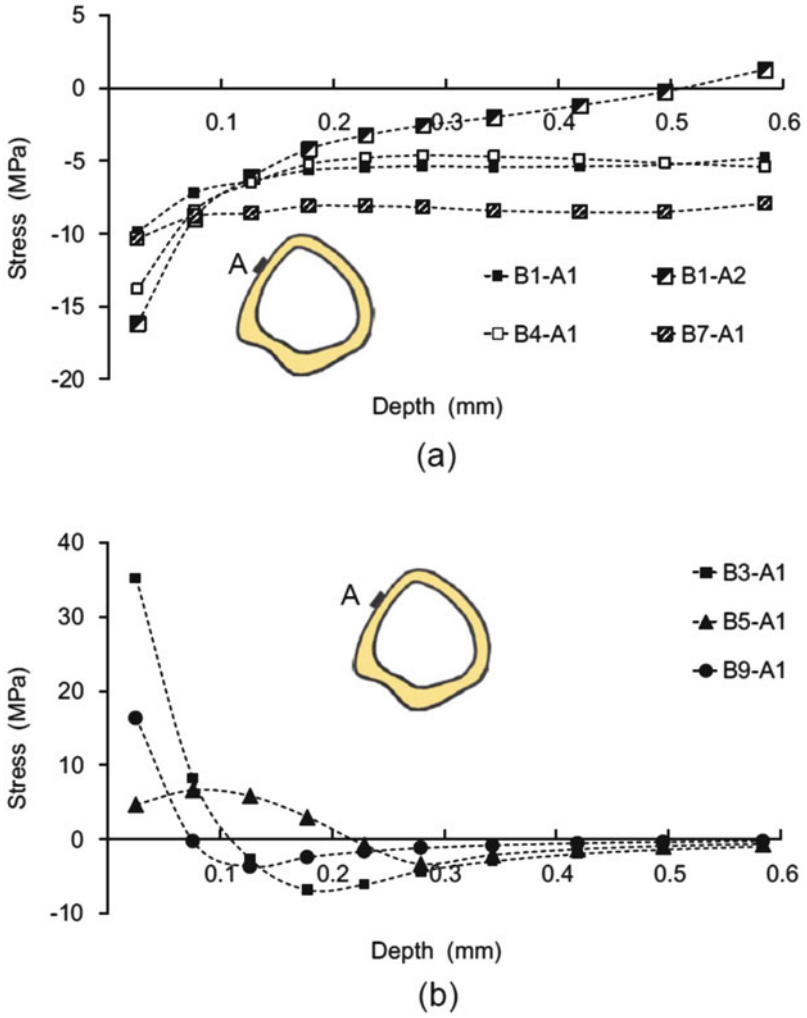

Fig. 1.7 Residual stresses vs. depth for (**a**) mature and (**b**) young femurs at location A

1.6 Discussion

Determination of residual stresses in layers near the surface may be of interest since fracture [47], fatigue [48, 49] and bone growth [50] mechanisms are prominent there.

The observation in this study of tensile residual stresses in surface layers of hydrated young femurs was not anticipated. An XRD study of young but air dried femurs [25] found minimal residual stresses at the surface (between about 0 and −10 MPa) and stresses that alternated between tension and compression (approx. +10 to −10 MPa depending on circumferential location) at depths between 0.5 and 3 mm. The unknown effect of air drying makes comparison with results observed here difficult. Maintaining hydration of larger bone specimens during XRD experiments can be challenging.

Bone is a microstructurally complex material [20]. An example is shown in Fig. 1.8, where the outer layers of a bovine femur have a lamellar structure like layers of bricks, while deeper layers have cylindrical osteons (Haversian structure). Residual stresses in this study represent values averaged over the volume of material removed by each step of slotting and may differ from values of residual stresses in smaller volumes.

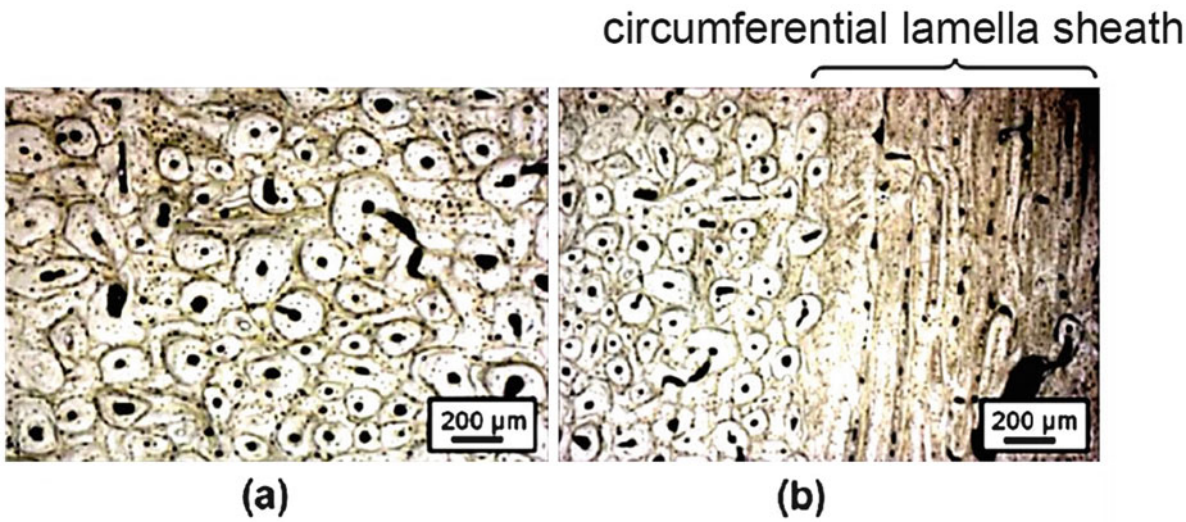

Fig. 1.8 Example showing (**a**) Haversian (osteons) and (**b**) lamellar microstructures (in circumferential sheath) of bovine femur, with micrographs from [44]

1.7 Conclusions

1. Development and application of a slotting method to find longitudinal residual stresses vs. depth in specimens of bone is feasible.
2. In hydrated bovine femurs from both mature and young animals, residual stresses were found to be greatest in thin layers near the surface, typically 100–200 μm deep.
3. In those layers, residual stresses in hydrated mature femurs were compressive at the circumferential location tested, but tensile in young femurs.

References

1. Fung, Y.: Biodynamics: Circulation, pp. 54–60. Springer, New York (1984)
2. Vishnav, R., Vossoughi, J.: Estimation of residual strains in aortic segments. In: Hall, C (ed.) Biomedical Engineering II, Recent Developments, pp 330–333. Pergamon Press, Elmsford, New York (1983)
3. Choung, C., Fung, Y.: On residual stresses in arteries. J. Biomech. Eng. **108**, 189–192 (1986)
4. Rachev, A., Greenwald, S.: Residual strains in conduit arteries. J. Biomech. **36**, 661–670 (2003)
5. Humphrey, J.: Cardiovascular Solid Mechanics: Cells, Tissues and Organs. Springer, New York (2002)
6. Holzapfel, G., et al.: Layer-specific 3D residual deformation of human aortas with non-atherosclerotic intimal thickening. Ann. Biomed. Eng. **35**, 530–545 (2007)
7. Gregersen, H., Lee, T., Chien, S., Skalak, R., Fung, Y.: Strain distribution in the layered wall of the esophagus. J. Biomech. Eng. **121**, 442–448 (1999)
8. Laio, F.Y., Zeng, G., Gregersen, H.: Stress distribution in the layered wall of the rat oesophagus. Med. Eng. Phys. **25**, 731–738 (2003)
9. Zhao, J., et al.: Opening angle and residual strain in a three-layered model of pig oesophagus. J. Biomech. **40**, 3187–3192 (2007)
10. Sokolis, D.: Strain-energy function and three-dimensional stress distribution in esophageal biomechanics. J. Biomech. **43**, 2753–2764 (2010)
11. Gao, C., Gregersen, H.: Biomechanical and morphological properties in rat large intestine. J. Biomech. **33**, 1089–1097 (2000)
12. Dou, Y., et al.: Longitudinal residual strain and stress-strain relationship in rat small intestine. Biomed. Eng. Online. **5**, 37 (2006). doi:10.1186/1475-925-5-37
13. Xu, G., Bayly, P., Taber, L.: Residual stress in the adult mouse brain. Biomech. Model. Mechanobiol. **8**, 253–262 (2009)

14. Matsumoto, T., Ikuta, N., Mori, M., Nagayam, K.: Mechanics of wrinkle formation: micromechanical analysis of skin deformation during wrinkle formation in ultraviolet-irradiated mice. Skin. Res. Tech. **16**, 179–189 (2010)
15. Fung, Y.: What are the residual stresses doing in our blood vessels? Ann. Biomed. Eng. **19**, 237–249 (1991)
16. Destrade, M., Liu, Y., Murphy, J., Kassab, G.: Uniform transmural strain in pre-stresses arteries occurs at physiological pressure. J. Theo. Biol. **303**, 93–97 (2012)
17. Delfino, A., Stergiopulos, N., Moore, J., Meister, J.: Residual strain effects on the stress field in a thick wall finite element model of the human carotid bifurcation. J. Biomech. **30**, 777–786 (1997)
18. Volokh, K.: Prediction of arterial failure based on microstructural bi-layer fiber-matrix model with softening. J. Biomech. **41**, 447–453 (2008)
19. Noyan, I., Cohen, J.: Residual Stress: Measurement by Diffraction and Interpretation. Springer, New York (1987)
20. Currey, J.: Bones: Structure and Mechanics. Princeton University Press, Princeton (2006)
21. Todoh, M., Tadano, S., Shibano, J., Ukai, T.: Polychromatic X-ray measurements of anisotropic residual stress in bone femoral bone. JSME Int. J. C. Mech. Sy. **43**, 795–801 (2000)
22. Singhal, A., Deymier-Black, A., Almer, J., Dunand, D.: Effect of high-energy X-ray doses on bone elastic properties and residual strains. J. Mech. Behav. Biomed. Mater. **4**, 1774–1786 (2011)
23. Yamada, S., Tadano, S.: Residual stress around the cortical surface in bovine femoral diaphysis. J. Biomech. Eng. **132**, 044503-1–044503-4 (2010)
24. Yamada, S., Tadano, S., Todoh, M., Fujisaki, K.: Residual stress distribution in the bovine femoral diaphysis measured by synchrotron. J. Biomech. Sci. Engr. **6**, 114–124 (2011)
25. Yamada, S., Tadano, S.: Effects of growth on residual stress distribution along the radial depth of cortical cylinders from bovine femurs. J. Biomech. **46**, 2130–2136 (2013)
26. Yamada, S., Tadano, S., Onuma, M.: X-ray diffraction technique with imaging plate for detecting surface distribution of residual stress in diaphysis of bovine femurs. Exp. Mech. **54**, 633–640 (2014)
27. Onuma, M., Yamada, S., Tadano, S.: Age-related residual stresses at diaphyseal surface of bovine femur measured by XRD-IP system. 15th Int. Conf. Biomed Eng, IFMBE Proc. **43**, 743–744 (2014)
28. Hoo, P., Fratrzl, P., Daniels, J., Dunlop, J., Honkimaki, V., Hoffman, M.: Cooperation of length scales and orientations in the deformation of bovine bone. Acta Biomater. **7**, 2943–2951 (2011)
29. Tung, P., Mudie, S., Daniels, J.: Hydration and radiation effects on the residual stress state of cortical bone. Acta Biomater. **9**, 9503–9507 (2013)
30. Almer, J., Stock, S.: Internal strains and stresses measured in cortical bone via high-energy X-ray diffraction. J. Struc. Biol. **152**, 14–27 (2005)
31. Almer, J., Stock, S.: Micromechanical response of mineral and collagen phases in bone. J. Struc. Biol. **157**, 365–370 (2007)
32. Tadano, S., Okoshi, T.: Residual stress in bone structure and tissue of rabbit's tibiofibula. Biomed. Mater. Eng. **16**, 11–21 (2006)
33. Yamada, S., Tadano, S., Fujisaki, K.: Residual stress distribution in rabbit limb bones. J. Biomech. **44**, 1285–1290 (2011)
34. Kotha, S., Guzelsu, N.: Effect of bone mineral content on the tensile properties of cortical bone: experiments and theory. J. Biomech. Eng. **125**, 785–793 (2003)
35. Currey, J.: What determines the bending strength of compact bone? J. Exp. Biol. **202**, 2495–2502 (1999)
36. Stanwyck, T., Fischer, R., Pope, M., Seligson, D.: Studies on prestress in bone. Biorheology. **19**, 301–306 (1982)
37. Prime, M.: Residual stress measurement by successive extension of a slot: the crack compliance method. Appl. Mech. Rev. **52**, 75–96 (1999)
38. Cheng, F., Finnie, I.: Residual Stress Measurement and the Slitting Method. Springer, New York (2007)
39. Hill, M.: Slitting (chap. 4). In: Schajer, G. (ed.) Practical Residual Stress Measurement Methods, pp. 89–108. Wiley, Chichester (2013)
40. Shokrieh, M., Akbari, A.: Measuring residual stress in composite materials, chap.5. In: Shokrieh, M. (ed.) Residual Stresses in Composite Materials. Woodhead Publishing, Cambridge, UK (2014)
41. Schajer, G., Prime, M.: Use of inverse solutions for residual stress measurements. J. Eng. Mater. Technol. **128**, 375–382 (2006)
42. Schajer, G.: Use of displacement data to calculate strain gauge response in non-uniform strain fields. Strain. **29**, 9–13 (1993)
43. Van Buskirk, W., Cowin, S., Ward, R.: Ultrasonic measurement of orthotropic elastic constants of bovine femoral bone. J. Biomech. Eng. **103**, 67–72 (1981)
44. Novitskaya, E., Chen, P., Lee, S., Castro-Cesena, A., Hiarta, G., Lubarda, V., McKittrick, J.: Anisotropy in the compressive mechanical properties of bovine cortical bone and the mineral and protein constituents. Acta Biomater. **7**, 3170–3177 (2011)
45. Manilay, Z., Novitskaya, E., Sadovnikov, E., McKittrick, J.: A comparative study of young and mature bovine cortical bone. Acta Biomater. **9**, 5280–5288 (2013)
46. Augustin, G., Zigman, T., Davila, S., Udilljak, T., Staroveski, T., Brezak, D., Babic, S.: Cortical bone drilling and thermal necrosis. Clin. Biomech. **27**, 313–325 (2012)
47. Gupta, H., Zioupos, P.: Fracture of bone tissue: the 'hows' and the 'whys'. Med. Eng. Phys. **30**, 1209–1226 (2008)
48. Kruzic, J., Ritchie, R.: Fatigue of mineralized tissues: cortical bone and dentin. J. Mech. Behav. Biomed. Mater. **1**, 3–17 (2008)
49. Yeni, Y., Fyhrie, D.: Fatigue damage-fracture mechanics interaction in cortical bone. Bone. **30**, 509–514 (2002)
50. Henderson, J., Carter, D.: Mechanical induction in limb morphogenesis: the role of growth-generated strains and prestress. Bone. **31**, 645–653 (2002)